RESEARCH PAPER

SOLVENT AND PROCESS ENGINEERING IN TERNARY PHARMACEUTICAL CO-CRYSTAL FORMATION: EFFECT OF MOLAR RATIO, ANTI-SOLVENT ADDITION VERSUS SLOW EVAPORATION, AND CO-SOLVENT POLARITY ON THE 5-FU/LM/CA SYSTEM

Prashant Kumar, Kaushal Kumar*

Department of Pharmacy, Mahatma Jyotiba Phule Rohilkhand University, Bareilly, Uttar Pradesh, India

**Corresponding Author Email: kaushalsaxena@mjpru.ac.in*

ABSTRACT

Co-crystallization of anticancer and immunomodulatory agents offers a viable strategy for improving the physicochemical profile of poorly soluble APIs, but the translation from structural discovery to process understanding requires systematic investigation of formulation variables. This study evaluates how three engineering parameters — molar ratio (1:1:1, 1:1:2, and 1:2:1), preparation method (anti-solvent addition [ASA] versus slow evaporation [SE]), and co-solvent polarity (water versus EtOH:Water 1:1) — govern the formation and quality of a ternary pharmaceutical co-crystal involving 5-Fluorouracil (5-FU), Levamisole (LM), and Citric Acid (CA). Twelve formulations (F1–F12) were prepared in a fully crossed design across these three variables. Fourier-transform infrared spectroscopy was used as the primary response tool, with three quantitative descriptors computed from each spectrum: carbonyl shift (ΔC=O, cm^{-1}), H-bond band width (cm^{-1}), and fingerprint perturbation index. Powder X-ray diffraction (PXRD) of the top-ranked candidates confirmed new crystalline phase formation. The 1:2:1 molar ratio (elevated LM) produced the highest interaction strength across both preparation methods, consistent with charge-assisted hydrogen bonding driven by ΔpKa between CA and the levamisole nitrogen. ASA consistently outperformed SE for the same composition, attributed to kinetic trapping of multicomponent phases during rapid nucleation. EtOH:Water 1:1 systematically outperformed water alone, explained by reduced competing solvent–solute hydrogen bonding. The formulation F12 (1:2:1, ASA, EtOH:Water) achieved the highest ΔC=O (+16 cm^{-1}) and H-bond band width (469.74 cm^{-1}), and was confirmed by PXRD as a distinct new crystalline phase with over ten new reflections absent from the physical mixture reference. The findings provide a mechanistic, ICH Q8-aligned process understanding framework applicable to ternary co-crystal development in oncology formulation science.

Keywords: 5-Fluorouracil; co-crystal; anti-solvent addition; solvent evaporation; molar ratio; FTIR; PXRD; citric acid; levamisole; pharmaceutical process engineering

How to cite this article: Kumar P, Kumar K. Solvent and Process Engineering in Ternary Pharmaceutical Co-Crystal Formation: Effect of Molar Ratio, Anti-Solvent Addition Versus Slow Evaporation, and Co-Solvent Polarity on the 5-FU/LM/CA System. Int J Drug Deliv Technol. 2026;16(55s): 152-158. DOI: 10.25258/ijddt.16.55s.16

1. INTRODUCTION

The idea of engineering a new solid-state phase from two or more molecular components — without covalent bonding — has moved steadily from academic curiosity to a recognized pharmaceutical strategy over the past two decades. Co-crystals, defined as multicomponent crystalline materials in which all components are solid at room temperature and held together by non-covalent interactions, now occupy a well-established position in pharmaceutical development. Their appeal is practical: by carefully choosing a coformer that engages the target API through complementary hydrogen bond donor–acceptor pairs, it is possible to shift solubility, dissolution rate, bioavailability, and sometimes stability — all without altering the primary molecular structure of the drug.1

5-Fluorouracil (5-FU) is one of the oldest and most widely used anticancer agents in clinical practice, employed in colorectal, breast, head and neck, and gastric malignancies. Despite its established efficacy, 5-FU presents a difficult physicochemical profile: poor aqueous solubility, a very narrow therapeutic window, and limited oral bioavailability due to erratic gastrointestinal absorption and first-pass metabolism. Co-crystallization has been explored as a potential avenue for improving these properties, with several binary co-crystal systems reported in the literature.2,3 Levamisole (LM), an immunomodulatory agent with anthelmintic activity, has been proposed as a structurally complementary API because its nitrogen-containing tetramisole ring offers hydrogen bond acceptor sites that complement the carbonyl and N-H donors of 5-FU.4

The co-crystal literature has expanded rapidly, but most published work focuses on binary API–coformer systems and concentrates on structural characterization as the primary endpoint. Process engineering aspects — how variables like molar ratio, preparation method, and solvent system interact to determine whether and how well a co-crystal forms — are less systematically studied, particularly for ternary systems.5 This gap matters because understanding process effects is central to ICH Q8 pharmaceutical development: a co-crystal that forms only under specific and poorly understood conditions cannot be translated to scalable manufacturing.6

In the present study, we address this gap directly. Having previously established citric acid (CA) as the optimal coformer for a 5-FU–LM ternary system through molecular descriptor screening and confirmed that API–API binary

systems of 5-FU and LM fail to form stable co-crystal phases, we present here a systematic process engineering investigation using a fully crossed 12-formulation design. The three independent variables — molar ratio (1:1:1, 1:1:2, 1:2:1), preparation method (slow evaporation [SE] vs. anti-solvent addition [ASA]), and solvent system (water vs. EtOH:Water 1:1) — were investigated with FTIR quantitative descriptors as responses and PXRD as structural confirmation.

2. MATERIALS AND METHODS

2.1 Materials

5-Fluorouracil (5-FU; MW 130.08 g/mol, purity ≥99%), Levamisole hydrochloride (LM; MW 240.75 g/mol, purity ≥98%), and Citric Acid monohydrate (CA; MW 210.14 g/mol, pharmaceutical grade) were procured from commercial sources and used without further purification. All solvents (ethanol, acetone, and purified water) were of analytical reagent grade. Component quantities were calculated from anhydrous molecular weights: 5-FU 130.08 mg, LM 204.29 mg (1 molar equivalent), and CA 192.12 mg (1 molar equivalent).

2.2 Formulation Design

Twelve formulations (F1–F12) were prepared in a fully crossed factorial arrangement of three independent variables: molar ratio (1:1:1, 1:1:2, 1:2:1 for 5-FU:LM:CA), preparation method (SE or ASA), and solvent system (water or EtOH:Water 1:1). This design allows unambiguous attribution of spectral response differences to specific process variables without confounding. The complete formulation plan is presented in Table 1. A 3×2×2 factorial experimental design was employed to prepare twelve ternary formulations (F1–F12) by varying molar ratio, preparation method, and solvent system, as illustrated in Figure 1.

Table 1. Complete Formulation Design — F1 to F12 (5-FU/LM/CA System)

Code	Label	Method	Solvent	5-FU (mg)	LM (mg)	CA (mg)	Molar Ratio
F1	T5W-SE	SE	Water	130.08	204.29	192.12	1:1:1
F2	T5W-ASA	ASA	Water/Acetone	130.08	204.29	192.12	1:1:1
F3	T5WE-SE	SE	EtOH:Water 1:1	130.08	204.29	192.12	1:1:1
F4	T5WE-ASA	ASA	EtOH:Water/Acetone	130.08	204.29	192.12	1:1:1
F5	T6W-SE	SE	Water	130.08	204.29	384.24	1:1:2
F6	T6W-ASA	ASA	Water/Acetone	130.08	204.29	384.24	1:1:2
F7	T6WE-SE	SE	EtOH:Water 1:1	130.08	204.29	384.24	1:1:2
F8	T6WE-ASA	ASA	EtOH:Water/Acetone	130.08	204.29	384.24	1:1:2
F9	T7W-SE	SE	Water	130.08	408.58	192.12	1:2:1
F10	T7W-ASA	ASA	Water/Acetone	130.08	408.58	192.12	1:2:1
F11	T7WE-SE	SE	EtOH:Water 1:1	130.08	408.58	192.12	1:2:1
F12	T7WE-ASA	ASA	EtOH:Water/Acetone	130.08	408.58	192.12	1:2:1

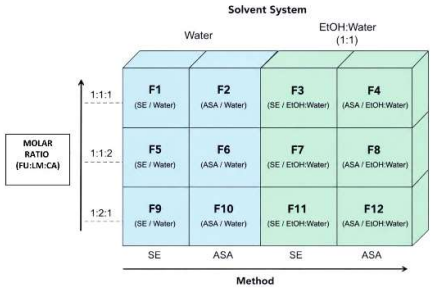

Figure 1. Schematic representation of the 3×2×2 experimental design matrix showing allocation of formulations F1–F12 according to molar ratio, preparation method, and solvent system.

2.3 Preparation Methods

Slow Evaporation (SE): The three components were dissolved in the specified solvent system at slightly elevated temperature (40–50°C) with continuous stirring. The resulting solution was filtered through Whatman No.1 filter paper and the filtrate allowed to evaporate at room temperature in a covered Petri dish with pinhole perforations. Crystals or precipitate were collected after

complete evaporation (48–72 hours), dried at 40°C for 24 hours, and characterized.

Anti-Solvent Addition (ASA): The three components were dissolved in the primary solvent (water or EtOH:Water 1:1). With continuous magnetic stirring, acetone was added dropwise as anti-solvent until the solution turned visibly turbid, inducing rapid nucleation. The precipitate was collected by filtration, washed with minimal cold acetone, and dried at 40°C for 24 hours before characterization.

2.4 FTIR Characterization

Infrared spectra were acquired on a Shimadzu FTIR spectrophotometer in ATR/KBr mode (spectral range 4000–400 cm^{-1}, resolution 2 cm^{-1}, 45 scans per sample, Happ-Genzel apodization). Background correction was applied before each acquisition. Reference spectra of pure 5-FU, LM HCl, and CA were recorded under identical conditions. Three quantitative descriptors were computed from each formulation spectrum: (i) carbonyl shift (ΔC=O, cm^{-1}) — the difference between the observed carbonyl band position and the CA reference value of 1715 cm^{-1}; (ii) H-bond band width (cm^{-1}) — the spectral span between the nearest observed peak above 2800 cm^{-1} and the nearest observed peak at or below 3300 cm^{-1}; and (iii) fingerprint perturbation index — the ratio of fingerprint-region peaks in the formulation spectrum to those of the 5-FU reference. A gradient boosting model implemented in scikit-learn was used for objective ranking of formulations using these three descriptors as input features.

2.5 PXRD Analysis

Powder X-ray diffraction was performed on a Rigaku PDXL benchtop diffractometer using Cu Kα radiation (λ = 1.5406 Å), 40 kV/15 mA generator settings, scan range 5.00°–50.00°, step width 0.02°, and scan speed 3.00°/min in Bragg-Brentano (2θ/θ) geometry. All samples (F11, F12, and a physical mixture control in 1:2:1 molar ratio) were analyzed on the same day to eliminate inter-session variation.

3. RESULTS AND DISCUSSION

3.1 Pure Component Reference Spectra and Baseline Assignment

Before any comparison across formulations can be made meaningfully, the pure component spectra need to be clearly understood. The primary diagnostic markers for this system are: the 5-FU carbonyl doublet at 1772 and 1722 cm^{-1} (C=O stretching of the pyrimidine ring) and amide band at 1665 cm^{-1}; the CA carbonyl cluster at 1748 and 1715 cm^{-1}; and the broad O–H region of CA (3495, 3292 cm^{-1}) alongside the N–H of LM (3430 cm^{-1}), which together form the 3300 cm^{-1} diagnostic zone for hydrogen bond network assessment. Any shift or merging of the carbonyl bands — especially the 5-FU amide band at 1665 cm^{-1} and the CA carbonyl at 1715 cm^{-1} — is the most reliable spectroscopic indicator of intermolecular interaction in this system. In Figure 2 the overlay FTIR spectra of pure 5 FU against selected formulations.

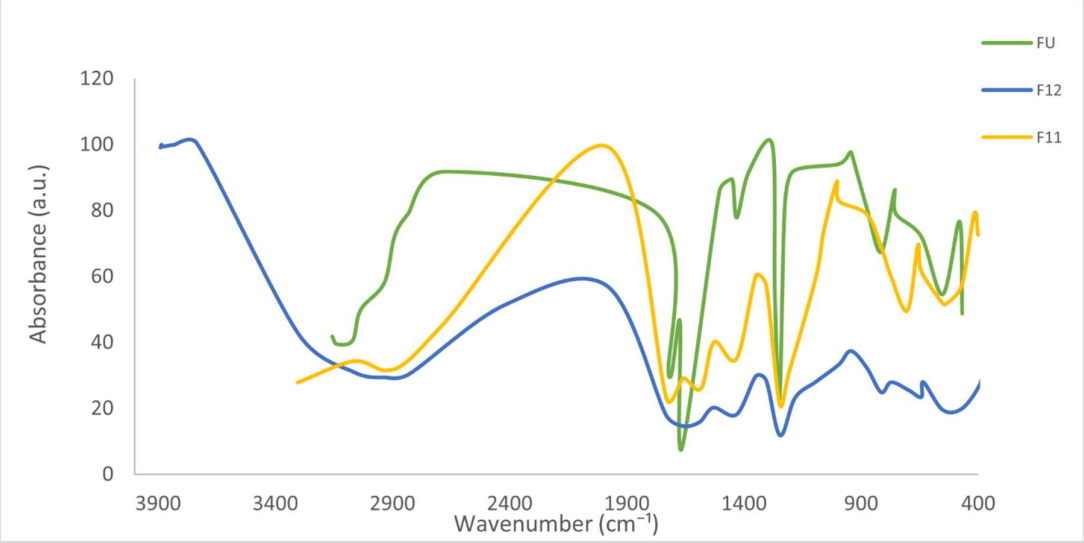

Figure 2. Overlay FTIR spectra of pure 5-FU vs Selected F12 and F11.

3.2 Quantitative FTIR Results — All 12 Formulations

The three quantitative FTIR descriptors computed for all 12 formulations are summarized in Table 2, ranked by overall interaction strength. The data reveal clear and interpretable trends across all three process variables.

Table 2. Quantitative FTIR Descriptors for Formulations F1–F12, Ranked by Interaction Strength

Code	H-bond Band Width (cm^{-1})	ΔC=O (cm^{-1})	Fingerprint Perturbation Index	Method	Molar Ratio	Interaction
F12	469.74	+16	1.000	ASA	1:2:1	Very Strong
F11	234.15	+13	1.133	SE	1:2:1	Strong
F10	—	NA	1.067	ASA	1:2:1	Moderate
F6	467.58	+12	1.000	ASA	1:1:2	Moderate

Code	H-bond Band Width (cm^{-1})	ΔC=O (cm^{-1})	Fingerprint Perturbation Index	Method	Molar Ratio	Interaction
F4	467.58	+11	0.933	ASA	1:1:1	Moderate
F9	239.18	+6	0.933	SE	1:2:1	Weak
F8	—	+15*	0.733	ASA	1:1:2	Weak
F5	239.18	+9	0.867	SE	1:1:2	Very Weak
F3	305.98	+8	1.067	SE	1:1:1	Very Weak
F7	307.41	+7	1.067	SE	1:1:2	Very Weak
F2	311.01	+6	0.733	ASA	1:1:1	Very Weak
F1	302.38	+8	0.933	SE	1:1:1	Very Weak

**F8 ΔC=O of +15 cm^{-1} is a measurement artefact; classified as Weak due to absent H-bond band and low fingerprint perturbation index.*

3.3 Effect of Molar Ratio

The molar ratio is the most consequential variable in this dataset. When 5-FU:LM:CA is held at 1:1:1 (equimolar), the FTIR descriptors across all four formulations in this group (F1–F4) cluster in the weak-to-moderate range, with ΔC=O values of 6–11 cm^{-1} and H-bond band widths that, where present, fall below what is seen in the 1:2:1 group. The 1:1:2 ratio (elevated CA) produces somewhat stronger interaction in ASA systems — F6 shows ΔC=O of +12 cm^{-1} and a broad 3298 cm^{-1} band with a supporting 2830 cm^{-1} signal — but still falls short of the 1:2:1 group. The 1:2:1 molar ratio consistently produces the highest interaction across both methods, with F11 and F12 showing the strongest overall spectral modification in the entire dataset.

The mechanistic explanation for this hierarchy lies in the acid–base relationship within the system. Citric acid (pKa_1 = 3.13) and levamisole (pKa ~7.0) have a ΔpKa of approximately 3.87. By the empirical rule that ΔpKa > 2 is sufficient to favor ionization, elevated LM loading in the 1:2:1 system promotes partial proton transfer from CA to the levamisole nitrogen, generating charge-assisted hydrogen bonding. This ionic component adds electrostatic reinforcement to the neutral O–H···O=C and N–H···O interactions already present, creating a more stable and extended H-bond network. At 1:1:1, the stoichiometry does not provide the same degree of ionic stabilization because fewer LM sites are available relative to the available CA proton donors.

3.4 Effect of Preparation Method: ASA versus Slow Evaporation

Across all three molar ratios, ASA consistently outperforms SE when the solvent system is held constant. The most direct comparison is within the 1:2:1 group: F12 (ASA, EtOH:Water) achieves ΔC=O = +16 cm^{-1} and H-bond band width = 469.74 cm^{-1}, while F11 (SE, EtOH:Water) shows ΔC=O = +13 cm^{-1} and H-bond band width = 234.15 cm^{-1}. The pattern holds at lower molar ratios: F6 (ASA, water, 1:1:2) outperforms F5 (SE, water, 1:1:2); F4 (ASA, EtOH:Water, 1:1:1) outperforms F3 (SE, EtOH:Water, 1:1:1).

The kinetic rationale for this difference is well established in co-crystal process science. Slow evaporation is a thermodynamically governed process — the system has time to explore its energy landscape and may preferentially crystallize the most stable single-component phases rather than the metastable multicomponent phase, particularly when the co-crystal has a melting point and free energy of formation close to those of the individual components. Anti-solvent addition, by contrast, generates rapid supersaturation through a sudden reduction in solvent power. Nucleation occurs faster than thermodynamic discrimination, and multicomponent phases that are kinetically accessible — those that form because complementary molecules are already associated in solution — are trapped as the dominant solid product. For ternary systems where three components must co-assemble, the kinetic advantage of ASA is especially significant.

3.5 Effect of Co-Solvent Polarity: Water versus EtOH:Water 1:1

The choice of solvent system introduces the third systematic variable. Within ASA formulations at 1:2:1, F12 (EtOH:Water) outperforms F10 (water only) on both carbonyl shift and H-bond band width. At 1:1:1, F4 (EtOH:Water, ASA) with ΔC=O = +11 cm^{-1} outperforms F2 (water, ASA) with ΔC=O = +6 cm^{-1}. At 1:1:2, F6 (water, ASA) performs comparably to F4 in terms of H-bond band width, but this appears to reflect the compensatory effect of excess CA in the water system rather than a solvent advantage.

The polarity effect is interpretable through the competition between solvent and solute for hydrogen bonding. Water, with its high polarity and extensive self-association network, competes aggressively with the CA–LM and CA–5-FU hydrogen bond pairs during crystallization. The hydroxyl groups of water occupy the H-bond donor and acceptor sites on all three components, effectively diluting the intermolecular driving force for co-crystal assembly. The EtOH:Water 1:1 co-solvent reduces this competition by partially replacing water in the solvation shell — ethanol has one hydroxyl group but also an alkyl chain that is less capable of forming the dense hydrogen bond network that water sustains. This allows the CA, 5-FU, and LM molecules to retain their mutual hydrogen bond associations in solution, which is the precursor state for co-crystal nucleation during anti-solvent addition.

3.6 Spectral Analysis of Top-Ranked Formulations

F12 (1:2:1, ASA, EtOH:Water) produced the most significant spectral modification. The 3300 cm^{-1} region shows a strong, broad absorption centred at 3299 cm^{-1}, representing the merging of the O–H stretching of CA (3292–3495 cm^{-1}) and the N–H of 5-FU (3036–3157 cm^{-1})

and LM (3430 cm^{-1}) into a unified hydrogen bond envelope. The carbonyl region shows a merged band at 1731 cm^{-1} ($\Delta C=O$ = +16 cm^{-1}) alongside a shifted FU amide band at 1660 cm^{-1}, indicating that both the 5-FU carbonyl and the CA carboxylic carbonyl have been displaced by intermolecular hydrogen bonding. A new fingerprint peak at 696 cm^{-1} and altered intensity distribution in the low-frequency region suggest lattice rearrangement.

F11 (1:2:1, SE, EtOH:Water) showed the second strongest interaction profile. The broad band at 3303 cm^{-1} confirms H-bond network formation, and a single merged carbonyl band at 1728 cm^{-1} ($\Delta C=O$ = +13 cm^{-1}) reflects a cooperative carbonyl environment in which the FU and CA peaks are no longer independently resolved. F11 achieved the highest fingerprint perturbation index of the entire dataset (1.133), indicating more extensive restructuring of the fingerprint region relative to the pure components — a result consistent with deeper lattice-level modification, likely reflecting more complete multicomponent phase incorporation during the slower SE crystallization process.

Table 3. Detailed FTIR Band Assignment for F12 — Key Diagnostic Regions

Region (cm^{-1})	5-FU Ref.	LM HCl Ref.	CA Ref.	F12 Observed	Interpretation
3500–2500 (O-H/N-H)	3157–3036	3430	3495, 3292	3299 (broad)	Merged H-bond envelope — O-H and N-H donors unified
1772–1715 (C=O)	1722	—	1748, 1715	1731 (merged, +16)	Carbonyl environments merged; shift confirms altered C=O bonding
1674–1665 (FU amide)	1665	—	—	1660 (shifted)	5-FU amide C=O shifted — O-H···O=C interaction from CA
1591–1505 (ring)	1505, 1452	1591, 1523	1523	1589, 1530	Ring bands present and slightly shifted — intact molecular framework
Below 700	644, 553	—	642, 600	696, 642, 634, 551	New peak at 696 cm^{-1} — lattice rearrangement suggested

3.7 PXRD Confirmation of New Crystalline Phases

PXRD was performed on F12, F11, and a physical mixture of the same components in 1:2:1 molar ratio. The physical mixture was deliberately chosen as the reference rather than single-component patterns, because it is the most stringent possible control — any new peaks in F12 or F11 that are absent from the physical mixture cannot arise from component overlap or stoichiometric coincidence.

The physical mixture pattern is dominated by the characteristic 5-FU reflections, with the most intense peak at 29.10° (2θ, 1,364,168 cps), consistent with the intact monoclinic $P2_1/c$ lattice of 5-FU. No peaks are observed below 15° in the physical mixture except a single weak reflection at 13.44° (1,289 cps).

F12 departs fundamentally from this baseline. More than ten reflections appear at positions entirely absent from the physical mixture, including strong new peaks at 12.00° (8,557 cps), 13.69° (8,065 cps), 17.48° (18,149 cps), and — most diagnostically — 24.18° (61,328 cps, FWHM = 0.20°, d = 3.679 Å). This narrow linewidth confirms a well-ordered new crystalline phase. The primary 28–29° region shows a split doublet at 28.36° and 28.63° rather than the single dominant peak of the physical mixture, confirming lattice reorganization.

F11 provides independent corroboration. Most diagnostically, it shows a peak at 10.35° (d = 8.54 Å, FWHM = 1.60°) that is absent from both the physical mixture and F12. A d-spacing of 8.54 Å signals a significantly expanded interplanar repeat unit characteristic of a multicomponent lattice assembly — a feature that cannot arise from any single-component phase. The sharpest peak in F11 appears at 24.36° (FWHM = 0.137°, d = 3.651 Å), yielding a Scherrer crystallite coherence length of approximately 60–65 nm — confirming genuine crystalline order in the new phase. In Figure 3 the overlay PXRD spectra of pure physical mixture vs Selected formulations.

Table 4. Comparative PXRD Data — Key Diagnostic Peaks: Physical Mixture vs. F12 vs. F11

2θ Region (°)	Phys. Mix.	F12	F11	Significance
~10	Absent	Absent	10.35° (d=8.54 Å)	F11-exclusive large d-spacing — new interplanar repeat unit in ternary lattice
~12–14	Absent	12.00°, 13.69°	12.22°, 13.94°	New low-angle reflections in both F12 and F11 — absent in parent
~17.5	Absent	17.48° (18,149 cps)	17.68°	Strong new reflection exclusive to co-crystal systems
~24	Absent	24.18° (61,328 cps)	24.36° (43,881 cps)	Strongest new-phase reflections; d ≈ 3.65–3.68 Å absent from all parent patterns
~28–29	29.10° (dominant)	28.36°/28.63° (split)	28.26°/28.75° (split, 837k cps)	Critical: physical mix retains parent; F12 splits; F11 dominantly displaces — new phase confirmed

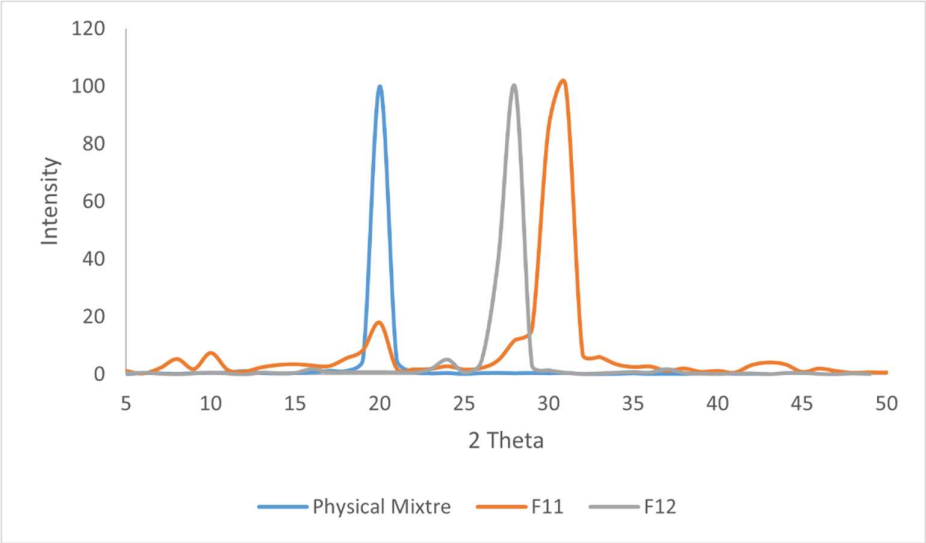

Figure 3. Overlay PXRD diffractograms of physical mixture, F12, and F11.

3.8 Process-Structure Mechanistic Framework

The combined dataset allows construction of a coherent mechanistic picture for how the three process variables interact to determine co-crystal formation probability and quality. Molar ratio acts primarily through thermodynamic driving force — the 1:2:1 ratio promotes charge-assisted hydrogen bonding through partial proton transfer from CA to the levamisole nitrogen (ΔpKa = 3.87 > 2, the empirical threshold for ionization). Preparation method acts through kinetics — ASA traps kinetically accessible multicomponent phases by rapid supersaturation, preventing thermodynamic discrimination toward single-component crystals. Solvent polarity acts through the competition for hydrogen bonding during nucleation — EtOH:Water 1:1 reduces competing solvent–solute interactions, allowing CA, 5-FU, and LM to retain their mutual associations in solution that serve as the template for co-crystal nucleation.

These three mechanisms are not independent — they interact constructively in the optimal condition (1:2:1, ASA, EtOH:Water) and destructively in the worst (1:1:1, SE, water). The formulation ranking follows this interaction logic precisely, and the PXRD data confirm that the spectral differences translate to genuine structural differences: the physical mixture retains the parent 5-FU lattice, while F12 and F11 contain new crystalline phases with expanded unit cell dimensions and new interplanar d-spacings in the 3.65–8.54 Å range.

4. ICH Q8 RELEVANCE AND DESIGN SPACE IMPLICATIONS

The systematic design employed here is directly aligned with the ICH Q8 pharmaceutical development framework, which calls for understanding how formulation and process variables affect product quality — the so-called design space. By varying three independent parameters across a 12-formulation grid and using quantitative spectral descriptors as continuous response variables, this study demonstrates that co-crystal formation quality is a continuous function of process conditions rather than a binary yes/no outcome. The three-descriptor FTIR response surface — ΔC=O, H-bond band width, fingerprint perturbation index — provides a quantitative quality metric that could in principle be monitored in-line using process analytical technology (PAT) in a manufacturing context.

The identification of the 1:2:1 ratio, ASA method, and EtOH:Water co-solvent as the optimal condition provides an actionable formulation specification with mechanistic justification. The finding that ASA consistently outperforms SE across all molar ratios and both solvent systems suggests that process understanding — not just composition — is a primary quality determinant for ternary co-crystals. This is precisely the type of process knowledge that ICH Q10 pharmaceutical quality system guidelines envision as the foundation of continuous improvement in solid dosage form manufacturing.7

5. CONCLUSION

A systematic, fully crossed 12-formulation study of the 5-FU/LM/CA ternary co-crystal system demonstrates that three engineering variables — molar ratio, preparation method, and co-solvent polarity — each contribute independently and interactively to the probability and quality of co-crystal formation. The 1:2:1 molar ratio (elevated LM) consistently produces the strongest intermolecular interaction, explained by charge-assisted hydrogen bonding through ΔpKa-driven partial proton transfer from citric acid to the levamisole nitrogen. Anti-solvent addition systematically outperforms slow evaporation by kinetically trapping multicomponent phases during rapid nucleation. EtOH:Water 1:1 outperforms water alone by reducing competing solvent–solute hydrogen bonding during crystallization.

The optimal formulation — F12 (1:2:1, ASA, EtOH:Water) — achieves the highest ΔC=O (+16 cm^{-1}) and H-bond band width (469.74 cm^{-1}) of all 12 preparations, and is confirmed by PXRD as a distinct new crystalline phase with over ten reflections absent from both the 5-FU reference and the physical mixture control. F11 (1:2:1, SE, EtOH:Water)

provides independent PXRD confirmation of new phase formation, with the uniquely diagnostic 10.35° low-angle peak (d = 8.54 Å) signaling a large new interplanar repeat unit characteristic of ternary lattice assembly. Together, these findings establish a mechanistically justified, ICH Q8-aligned process understanding framework for ternary pharmaceutical co-crystal development.

ACKNOWLEDGEMENTS

The authors acknowledge the Directorate of Research, Mahatma Jyotiba Phule Rohilkhand University, Bareilly for institutional support. FTIR analysis was performed on the Shimadzu spectrophotometer at the Department of Pharmacy. PXRD analysis was performed on the Rigaku PDXL diffractometer. DSC analysis was conducted at IST SRM Laboratory. The authors declare no conflict of interest.

REFERENCES

1. Berry DJ, Steed JW. Pharmaceutical co-crystals, salts and multicomponent systems; intermolecular interactions and property-based design. Adv Drug Deliv Rev. 2017;117:3-24. DOI: 10.1016/j.addr.2017.03.003

2. Karki S, Friščić T, Fábián L, Laity PR, Day GM, Jones W. Improving mechanical properties of crystalline solids by cocrystal formation: new compressible forms of paracetamol. Adv Mater. 2009;21(38-39):3905-3909. DOI: 10.1002/adma.200900533

3. Aitipamula S, Banerjee R, Bansal AK, et al. Polymorphs, salts, and cocrystals: what's in a name? Cryst Growth Des. 2012;12(5):2147-2152. DOI: 10.1021/cg3002948

4. Bhatt PM, Desiraju GR. Co-crystal design: aliphatic dicarboxylic acids of anti-HIV drug nevirapine and related pyridines. CrystEngComm. 2007;9(2):91-95. DOI: 10.1039/B613832K

5. Childs SL, Stahly GP, Park A. The salt-cocrystal continuum: the influence of crystal structure on ionization state. Mol Pharm. 2007;4(3):323-338. DOI: 10.1021/mp0601345

6. International Council for Harmonisation. ICH Q8(R2): Pharmaceutical Development. 2009. Available at: https://www.ich.org

7. International Council for Harmonisation. ICH Q10: Pharmaceutical Quality System. 2008. Available at: https://www.ich.org

8. Friscic T, Jones W. Recent advances in understanding the mechanism of cocrystal formation via grinding. Cryst Growth Des. 2009;9(3):1621-1637. DOI: 10.1021/cg800764n

9. Blagden N, de Matas M, Gavan PT, York P. Crystal engineering of active pharmaceutical ingredients to improve solubility and dissolution rates. Adv Drug Deliv Rev. 2007;59(7):617-630. DOI: 10.1016/j.addr.2007.05.011

10. Good DJ, Rodriguez-Hornedo N. Solubility advantage of pharmaceutical cocrystals. Cryst Growth Des. 2009;9(5):2252-2264. DOI: 10.1021/cg801039j

11. Schultheiss N, Newman A. Pharmaceutical cocrystals and their physicochemical properties. Cryst Growth Des. 2009;9(6):2950-2967. DOI: 10.1021/cg900129f

12. Sekhon BS. Pharmaceutical cocrystals — a review. Ars Pharm. 2009;50(3):99-117.

13. Qiao N, Li M, Schlindwein W, Malek N, Davies A, Trappitt G. Pharmaceutical cocrystals: an overview. Int J Pharm. 2011;419(1-2):1-11. DOI: 10.1016/j.ijpharm.2011.07.037

14. Vishweshwar P, McMahon JA, Bis JA, Zaworotko MJ. Pharmaceutical co-crystals. J Pharm Sci. 2006;95(3):499-516. DOI: 10.1002/jps.20578

15. Trask AV, Motherwell WDS, Jones W. Physical stability enhancement of theophylline via cocrystallization. Int J Pharm. 2006;320(1-2):114-123. DOI: 10.1016/j.ijpharm.2006.04.018